Research Article | Vol. 25, No. 1 | 9 Jan 2017 | OPTICS EXPRESS 486

Optics EXPRESS

Quasi-continuous frequency tunable terahertz quantum cascade lasers with coupled cavity and integrated photonic lattice

IMAN KUNDU,* PAUL DEAN, ALEXANDER VALAVANIS, LI CHEN, LIANHE LI, JOHN E. CUNNINGHAM, EDMUND H. LINFIELD, AND A. GILES DAVIES

School of Electronic and Electrical Engineering, University of Leeds, Leeds LS2 9JT, UK
**i.kundu@leeds.ac.uk*

Abstract: We demonstrate quasi-continuous tuning of the emission frequency from coupled cavity terahertz frequency quantum cascade lasers. Such coupled cavity lasers comprise a lasing cavity and a tuning cavity which are optically coupled through a narrow air slit and are operated above and below the lasing threshold current, respectively. The emission frequency of these devices is determined by the Vernier resonance of longitudinal modes in the lasing and the tuning cavities, and can be tuned by applying an index perturbation in the tuning cavity. The spectral coverage of the coupled cavity devices have been increased by reducing the repetition frequency of the Vernier resonance and increasing the ratio of the free spectral ranges of the two cavities. A continuous tuning of the coupled cavity modes has been realized through an index perturbation of the lasing cavity itself by using wide electrical heating pulses at the tuning cavity and exploiting thermal conduction through the monolithic substrate. Single mode emission and discrete frequency tuning over a bandwidth of 100 GHz and a quasi-continuous frequency coverage of 7 GHz at 2.25 THz is demonstrated. An improvement in the side mode suppression and a continuous spectral coverage of 3 GHz is achieved without any degradation of output power by integrating a π-phase shifted photonic lattice in the laser cavity.

OCIS codes: (140.5965) Semiconductor lasers, quantum cascade; (140.3570) Lasers, single-mode; (140.3600) Lasers, tunable.

References and Links

1. R. Köhler, A. Tredicucci, F. Beltram, H. E. Beere, E. H. Linfield, A. G. Davies, D. A. Ritchie, R. C. Iotti, and F. Rossi, "Terahertz semiconductor-heterostructure laser," Nature **417**(6885), 156–159 (2002).
2. G. Scalari, C. Walther, M. Fischer, R. Terazzi, H. Beere, D. Ritchie, and J. Faist, "THz and sub-THz quantum cascade lasers," Laser Photonics Rev. **3**(1-2), 45–66 (2009).
3. L. Li, I. Kundu, P. Dean, E. H. Linfield, and A. G. Davies, "High-power GaAs/AlGaAs quantum cascade lasers with emission in the frequency range 4.7–5.6 THz," in *International Quantum Cascade Lasers School and Workshop* (2016).
4. L. Li, L. Chen, J. Zhu, J. Freeman, P. Dean, A. Valavanis, A. G. Davies, and E. H. Linfield, "Terahertz quantum cascade lasers with >1 W output powers," Electron. Lett. **50**(4), 309–311 (2014).
5. S. Fathololoumi, E. Dupont, C. W. I. Chan, Z. R. Wasilewski, S. R. Laframboise, D. Ban, A. Mátyás, C. Jirauschek, Q. Hu, and H. C. Liu, "Terahertz quantum cascade lasers operating up to ~ 200 K with optimized oscillator strength and improved injection tunneling," Opt. Express **20**(4), 3866–3876 (2012).
6. M. Tonouchi, "Cutting-edge terahertz technology," Nat. Photonics **1**(2), 97–105 (2007).
7. H.-W. Hübers, S. G. Pavlov, H. Richter, A. D. Semenov, L. Mahler, A. Tredicucci, H. E. Beere, and D. A. Ritchie, "High-resolution gas phase spectroscopy with a distributed feedback terahertz quantum cascade laser," Appl. Phys. Lett. **89**(6), 061115 (2006).
8. P. Dean, Y. L. Lim, A. Valavanis, R. Kliese, M. Nikolić, S. P. Khanna, M. Lachab, D. Indjin, Z. Ikonić, P. Harrison, A. D. Rakić, E. H. Linfield, and A. G. Davies, "Terahertz imaging through self-mixing in a quantum cascade laser," Opt. Lett. **36**(13), 2587–2589 (2011).
9. H. W. Hubers, "Terahertz Heterodyne Receivers," IEEE J. Sel. Top. Quantum Electron. **14**(2), 378–391 (2008).
10. M. S. Vitiello and A. Tredicucci, "Tunable Emission in THz Quantum Cascade Lasers," IEEE Trans. Terahertz Sci. Technol. **1**(1), 76–84 (2011).

#279895 http://dx.doi.org/10.1364/OE.25.000486
Journal © 2017 Received 2 Nov 2016; revised 26 Nov 2016; accepted 30 Nov 2016; published 6 Jan 2017

Optics EXPRESS

11. D. Turčinková, M. I. Amanti, F. Castellano, M. Beck, and J. Faist, "Continuous tuning of terahertz distributed feedback quantum cascade laser by gas condensation and dielectric deposition," Appl. Phys. Lett. **102**(18), 181113 (2013).
12. N. Han, A. de Geofroy, D. P. Burghoff, C. W. I. Chan, A. W. M. Lee, J. L. Reno, and Q. Hu, "Broadband all-electronically tunable MEMS terahertz quantum cascade lasers," Opt. Lett. **39**(12), 3480–3483 (2014).
13. D. Turčinková, M. I. Amanti, G. Scalari, M. Beck, and J. Faist, "Electrically tunable terahertz quantum cascade lasers based on a two-sections interdigitated distributed feedback cavity," Appl. Phys. Lett. **106**(13), 131107 (2015).
14. F. Castellano, V. Bianchi, L. Li, J. Zhu, A. Tredicucci, E. H. Linfield, A. Giles Davies, and M. S. Vitiello, "Tuning a microcavity-coupled terahertz laser," Appl. Phys. Lett. **107**(26), 261108 (2015).
15. M. Hempel, B. Röben, L. Schrottke, H.-W. Hübers, and H. T. Grahn, "Fast continuous tuning of terahertz quantum-cascade lasers by rear-facet illumination," Appl. Phys. Lett. **108**(19), 191106 (2016).
16. K. Boylan, V. Weldon, D. McDonald, J. O'Gorman, and J. Hegarty, "Sampled grating DBR laser as a spectroscopic source in multigas detection at 1.52-1.57 μm," IEE Proc., Optoelectron. **148**(1), 19–24 (2001).
17. I. Kundu, P. Dean, A. Valavanis, L. Chen, L. Li, J. E. Cunningham, E. H. Linfield, and A. G. Davies, "Discrete Vernier tuning in terahertz quantum cascade lasers using coupled cavities," Opt. Express **22**(13), 16595–16605 (2014).
18. L. A. Coldren, S. W. Corzine, and M. L. Masanovic, *Diode Lasers and Photonic Integrated Circuits*, Second, Wiley Series in Microwave and Optical Engineering (John Wiley & Sons, 2012).
19. L. A. Coldren, "Monolithic tunable diode lasers," IEEE J. Sel. Top. Quantum Electron. **6**(6), 988–999 (2000).
20. S. Chakraborty, T. Chakraborty, S. P. Khanna, E. H. Linfield, A. G. Davies, J. Fowler, C. H. Worrall, H. E. Beere, and D. A. Ritchie, "Spectral engineering of terahertz quantum cascade lasers using focused ion beam etched photonic lattices," Electron. Lett. **42**(7), 404–405 (2006).
21. I. Kundu, P. Dean, A. Valavanis, L. Li, Y. Han, E. H. Linfield, and A. G. Davies, School of Electronic and Electrical Engineering, University of Leeds, Woodhouse Lane, Leeds LS2 9JT, U.K. are preparing a manuscript to be called "Frequency tunability and spectral control in terahertz quantum cascade lasers with phase adjusted finite defect site photonic lattice."
22. I. Kundu, P. Dean, A. Valavanis, L. Chen, L. H. Li, J. E. Cunningham, E. H. Linfield, and A. G. Davies, "Dataset associated with Quasi-continuous frequency tunable terahertz quantum cascade lasers with coupled cavity and integrated photonic lattice," University of Leeds data repository (2016) http://doi.org/10.5518/115.
23. H. Li, J. C. Cao, Y. J. Han, Z. Y. Tan, and X. G. Guo, "Temperature profile modelling and experimental investigation of thermal resistance of terahertz quantum-cascade lasers," J. Phys. Appl. Phys. **42**(20), 205102 (2009).
24. Paul Harrison and Alexander Valavanis, *Quantum Wells, Wires and Dots - Theoretical and Computational Physics of Semiconductor Nanostructures*, Fourth Edition (John Wiley & Sons, 2015).
25. COMSOL AB, *COMSOL Multiphysics (R) Version 4.4 - Heat Transfer Module User's Guide* (2013).
26. C. Worrall, J. Alton, M. Houghton, S. Barbieri, H. E. Beere, D. Ritchie, and C. Sirtori, "Continuous wave operation of a superlattice quantum cascade laser emitting at 2 THz," Opt. Express **14**(1), 171–181 (2006).
27. J. Carroll, J. Whiteaway, and D. Plumb, *Distributed Feedback Semiconductor Lasers*, Circuits, Devices and Systems Series No. 10 (The Institution of Electrical Engineers, London, 1998).

1. Introduction

Terahertz (THz) frequency quantum cascade lasers (QCLs) are compact unipolar semiconductor sources of THz radiation in which photons are generated through inter-subband transitions. Since their first demonstration in 2002 [1], these devices have undergone remarkable development and can now cover a broad spectral range between ~1.2–5.6 THz [2,3], with peak output powers of up to 1 W [4] and a maximum operating temperature of ~200 K [5] demonstrated.

THz QCL ridge waveguides are essentially Fabry–Pérot (FP) etalons that support multiple longitudinal modes. However, for many practical applications, including astronomical observations [6], gas spectroscopy [7], self-mixing interferometry [8], and heterodyne mixing [9], a single mode and frequency-tunable THz source is desirable. Frequency tuning in these devices has been demonstrated previously using external cavities [10], gas condensation [11], microelectromechanical system actuators [12], inter-digitated distributed feedback cavities [13], micro-cavity coupled mirrors [14], and facet illumination [15]. Notably, electrical tuning mechanisms commonly exploited in visible and near-infrared diode lasers are impractical for THz QCLs since the underlying electron plasma and band-filling effects responsible for control of the refractive index are much weaker in intersubband lasers [16], and become increasingly weak with decreasing frequency. Thermally-induced index perturbations can be exploited in THz QCLs through control of either the injected current or heat sink temperature,

Optics EXPRESS

although current tuning is typically only ~–5 MHz/mA—one order of magnitude smaller than in mid-IR QCLs [10]. Moreover, the sensitivity of THz QCL operation to temperature can result in significant variation of output power when thermal tuning is employed. As such, the design of an electrically controlled, wideband frequency-tunable THz QCL remains a technological challenge.

We recently demonstrated THz QCLs with an electrically-controlled frequency tunability by exploiting Vernier selection and localized Joule heating in a monolithically integrated coupled cavity (CC) [Fig. 1(a)], which was defined post-packaging using focused-ion beam (FIB) milling [17]. In such devices one of the cavities forms the active lasing cavity, whereas the other forms the passive tuning cavity. The CC mode that corresponds to the strongest Vernier alignment between modes of the individual reflectivity combs associated with the different cavity sections experiences the lowest lasing threshold [Fig. 1(b)]. As a result, lasing is selectively favored at this CC mode (the '*resonant CC mode'*). Mode selection in such two-section lasers therefore depends on the free spectral range (FSR) and the specific longitudinal modes of the constituent cavities [18]. Whilst these Vernier resonance frequencies are periodic and repeat after a *repetition frequency*, our previous CC QCLs were designed such that these repetition frequencies were outside the gain bandwidth of the QCL. Furthermore, in these devices a controlled index perturbation applied to either of the two cavities can shift the mode alignment to a different CC mode, resulting in discrete frequency tuning (i.e., a mode hop). The CC QCLs reported previously were optimized to achieve such discrete frequency tuning through Joule heating of one of the cavities. However, *continuous* frequency coverage between mode hops was not observed in these structures due to the absence of any index perturbation applied to the lasing cavity itself. We note that continuous frequency tuning based on Vernier selection has been studied in diode lasers based on sampled grating distributed feedback (SG-DBR) structures [19]. In such SG-DBR lasers the resonant CC mode can be tuned continuously by perturbing both reflectivity combs concurrently and through the use of additional waveguide sections to satisfy phase matching conditions [16]. However, direct scaling of SG-DBR designs to THz CC QCLs would require the waveguides to be tens of millimeters long and would therefore demand impractically large operating currents.

In this work, we extend the CC THz QCL concept to achieve more complete spectral coverage by increasing the number of accessible CC modes within the gain bandwidth (F_{gain}) of our devices, and also by introducing mechanisms for applying an index perturbation to the lasing cavity to enable continuous tuning of the CC modes. The former is achieved through careful selection of various design aspects of CC lasers: first, by increasing the FSR of the tuning cavity (F_t) resulting in an increase in the comb spacing ratio, CSR (CSR = F_t/F_l, where F_l is the FSR of the lasing cavity); second, by reducing the repetition frequency (F_r) of Vernier alignment of the CC modes such that $F_{gain}<F_r<1.5\ F_{gain}$; and lastly, by selection of cavity lengths that allow mode hops with both red and blue shifts in frequency. Unlike previous CC devices where the mode hops were strictly red or blue shifts with a frequency separation between the mode hops $\Delta F \sim F_t$, these design modifications allow ΔF to vary as a function of index perturbation, thereby increasing the number of accessible CC modes. At the same time, continuous tuning of the CC modes is achieved through a combination of approaches: first, by varying the drive current in the lasing cavity directly; and, second, by varying the duty cycle of the current pulses applied to the tuning cavity (up to 95% duty cycle), which results in thermal perturbation of the lasing section via heat conduction through the monolithic substrate. Using the thermal perturbation in the lasing cavity, in conjunction with controlled discrete frequency tuning between CC modes, we therefore accomplish a scheme for *quasi-continuous* tuning in these CC QCL devices. Discrete frequency tuning is demonstrated over 2.185–2.285 THz with a continuous tuning over ~4.5 GHz and quasi-continuous tunability ~7 GHz, around ~2.25 THz. Furthermore, in order to improve the side mode suppression ratio (SMSR) achieved with these devices, finite defect sites are

Optics EXPRESS

incorporated in the laser cavity to form a one-dimensional photonic lattice with a central π-phase defect [20,21]. Continuous frequency tuning of a single CC mode (SMSR: 40 dB) is then achieved over ~3 GHz, without any degradation in output power.

2. Device design

Resonant modes corresponding to Vernier alignment in CC lasers are separated by $F_r \sim NF_1F_2/\delta$, where F_1 and F_2 are the FSRs of the two cavities such that $F_1<F_2$, $N = F_2/F_1$ (rounded to the nearest integer), and δ is the remainder of F_2/F_1. As such, in order to eliminate the risk of two-color/multi-mode emission, CC lasers are typically designed such that the repetition frequency is larger than the gain bandwidth of the active region. When an index perturbation is applied to either of the two cavities, the Vernier alignment hops to a different CC mode that corresponds with the adjacent mode of the cavity with the larger FSR (i.e. F_2). In such devices, $\Delta F \sim F_2$, and the number of accessible CC modes is limited to $\sim F_{gain}/F_2$. We note that the number of accessible modes can be increased, and continuous tuning over F_{gain} is possible in a CC design with $N = 1$ simply by increasing the cavity lengths (i.e. reducing the FSR). However, scaling such a design to THz frequencies is limited by the narrow current and temperature tunability of THz QCLs, and would require individual cavities to be ~7–8 mm long (FSR~5–6 GHz). Furthermore, the low facet reflectivity associated with single metal THz QCLs results in CC combs with low finesse, which can lead to multi-mode emission from such long CC devices.

Instead, in order to increase the number of accessible CC modes, we designed a CC QCL with $1<F_r/F_{gain}<1.5$ (F_r/F_{gain} was arbitrarily selected to be ~1.3) and a high CSR (>2.5). The cavity lengths were selected such that, by applying an index perturbation to the tuning cavity, the resonant CC modes can hop controllably to CC modes corresponding to Vernier alignment with adjacent modes in either the lasing cavity (for which $\Delta F \sim F_l$) or the tuning cavity (for which $\Delta F \sim F_t$). Furthermore, an additional index perturbation applied to the *lasing* cavity in these devices can enable continuous tuning of the CC modes. By exploiting both of these mechanisms in combination, the number of accessible emission frequencies from our CC QCLs can be increased whilst also enabling controllable quasi-continuous tuning between them.

2.1 Coupled cavity design with a high comb spacing ratio

To this end, we designed a CC THz QCL with a 3.52-mm-long lasing cavity (FSR, F_l = 11.9 GHz) and a 1.29-mm-long tuning cavity (FSR, F_t = 32.2 GHz), separated by an air gap of 16.7 μm, i.e. with F_r~137 GHz and a CSR = 2.7. The spectral performance of the device was modelled using a transfer matrix approach as described in Refs [17,18]. In the first instance, the CC modes supported by the device were calculated as the refractive index was varied in the tuning cavity only. As shown in Fig. 1(b) and included in Dataset 1 [22], the device supports CC modes with F_r~137 GHz (frequency separation between modes 3 and 1') that hop (red-shift) sequentially in steps of ΔF~35 GHz (~F_t) as the refractive index is varied (i.e. modes 1-2-3 and 1'-2'-3′). Unlike our previous CC devices where cavity lengths were selected to enable mode hops with $\Delta F \sim F_t$ (analogous to modes 1-2-3), the cavity lengths and the lower F_r in the present design allows two concurrent mode hop regimes to exist as the refractive index in the tuning cavity is varied. Whilst a low repeat frequency can result in the presence of multiple resonant CC modes (for example, modes 3 and 1'), which could potentially result in dual-mode emission under certain conditions, we note that this value is just below F_{gain}~110 GHz (centered at ~2.25 THz), i.e. F_r/F_{gain}~1.25. Hence, the frequency-dependent gain of the material can be used to suppress such dual-mode emission. It is also evident that this design not only allows discrete tuning to CC modes corresponding to Vernier alignment with adjacent modes in the tuning cavity (for example, modes 1 and 2, for which $\Delta F \sim F_t$), but also adjacent modes in the lasing cavity (for example, mode 1 and 3′, for which $\Delta F \sim F_l$). Additionally, as is evident from Fig 1(b), a range of mode hops between resonant CC

Optics EXPRESS

modes with different frequency separations are possible in this device as the refractive index of the tuning cavity is varied, specifically: ΔF ~–35 GHz [modes 1-2-3 and 1'-2'-3′], ΔF ~–23 GHz [modes 1-2'], and ΔF ~59 GHz [modes 1-1' and 2-2']. Hence, this design increases the number of accessible spectral lines falling within the bandwidth of the device compared to the previous design [17]. We also note that this design results in slightly 'off-resonance' CC modes (for example modes A, B, C and D) at frequencies for which the reflectivity combs of the lasing and tuning cavities only align partially. Whilst the presence of such modes risks undesirable multiple mode emission, they can also be exploited in our tuning scheme; by introducing an index perturbation to the *lasing* cavity, Vernier alignment between these modes and modes of the tuning cavity can be achieved, resulting in a resonant CC mode. This allows a further increase in the number of accessible spectral lines in our device, as well as providing a mechanism to tune the CC modes continuously, as explained in Section 2.2.

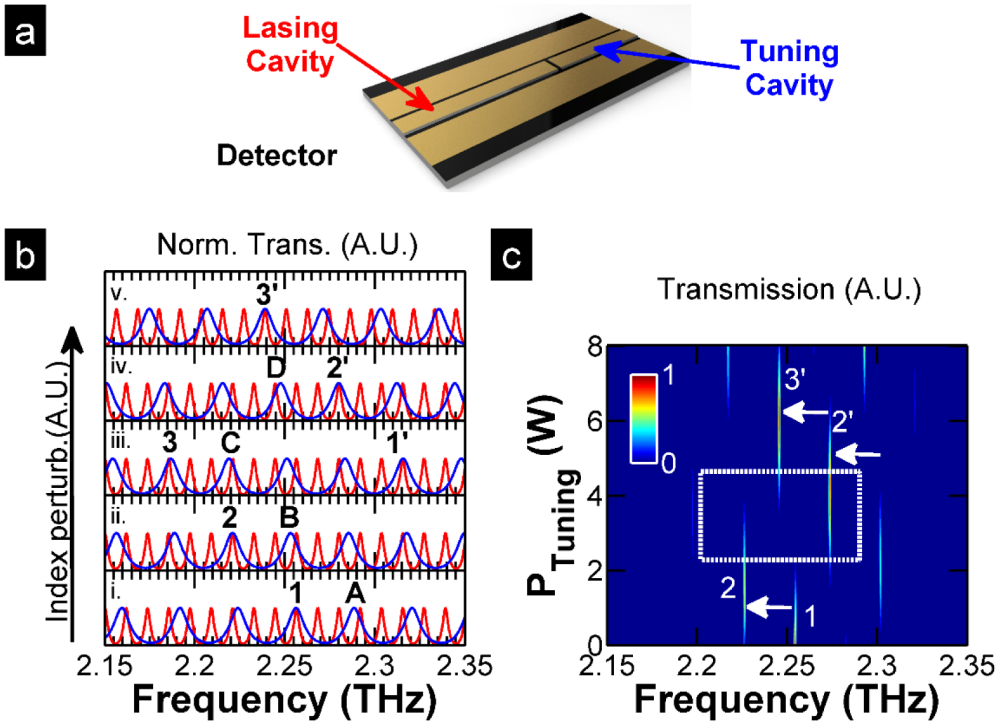

Fig. 1. (a) Schematic diagram of a CC THz QCL. (b) Illustration of Vernier selection in a CC THz QCL with a F_r~137 GHz and CSR of 2.7. Normalized transmission in the lasing (red) and the tuning (blue) cavities are shown as the index is varied in: (i-iv) the tuning cavity only, and (v) both cavities. The resonant CC modes are marked as 1 to 3 and 1' to 3′, and the off-resonance modes are marked as A to D. (c) Simulated transmission and discrete tuning (mode hopping) when the lasing cavity is driven with 2-μs-wide pulses (P_{Lasing} = 4.5 W) as a function of P_{Tuning} (10-μs-wide pulses). Mode transitions from mode 1 through to mode 3′ are marked. Modes 1 and 3′ are separated by ~11 GHz.

In order to simulate the behavior of our CC design as a function of peak electrical heating power supplied to the tuning cavity (P_{Tuning}), a thermal resistance of 20.5 KcmW^{-1}, calculated following the procedure described by Li et al in [23], and a tuning coefficient of $dn/dT = 9.5 \times 10^{-5}$ K^{-1} [17], were used in the transfer matrix model. As shown in Fig. 1(c), this predicts discrete tuning between resonant CC modes at frequencies 2.254, 2.225, 2.270 and 2.245 THz [analogous to modes 1, 2, 2', and 3′ in Fig. 1(b)] as P_{Tuning} (10-μs-wide current pulses) is increased. Although modes 1-2-3 or 1'-2'-3′ red shift in frequency [Fig. 1(b)], a blue shift (modes 2-2') is simulated at P_{Tuning}~2-4 W [Fig. 1(c)]. This is due to the low F_r/F_{gain} and the

Optics EXPRESS

cavity lengths used in this design. By inspection, the CC modes 1 and 3′ can be identified as corresponding to Vernier alignment with adjacent modes of the longer lasing cavity, with a frequency separation of $F_1 \approx 11$ GHz. Through also applying a controlled index perturbation to the *lasing* cavity, it is expected that both of these modes can be tuned *continuously* to improve the spectral coverage of the device further.

2.2 Index perturbation in the lasing cavity

In order to perturb the refractive index of the lasing cavity, the current amplitude supplied to this section can be varied. However, the index perturbation achievable by this approach alone is limited by the operating dynamic range of the device. Hence, in our scheme we supplied wide current pulses to the tuning cavity, and exploited the thermal conduction through the monolithic substrate to introduce an additional index perturbation in the lasing cavity. As such, continuous current pulse trains (10 kHz) with pulse widths varied in the range 20–95 μs were supplied to the tuning cavity, whilst the lasing cavity was driven using a constant 2-μs-wide pulse train (also at 10 kHz). These pulse trains were synchronized such that the pulses switched off simultaneously, as shown in Fig. 2(a). The electrical heating power supplied to the tuning section was calculated from the current–voltage relationship obtained experimentally.

In order to understand and calibrate the thermal coupling between the lasing and tuning cavities, the following time-dependent equation based on the Fourier law of heat conduction was solved,

$$\rho c_{\mathrm{p}}(T,T_{\mathrm{D}})\frac{\partial T}{\partial t} = \nabla\cdot\left[\kappa(T)\nabla T\right] + Q(t) \qquad (1)$$

where ρ is the material density, $Q(t)$ is the input electric power density, T is the temperature, $\kappa(T)$ is the temperature dependent thermal conductivity and $c_{\mathrm{p}}(T,T_{\mathrm{D}})$ is the temperature dependent specific heat capacity of the material as a function of Debye temperature (T_{D}). Temperature dependent material parameters were used to model the CC devices, as described by Harrison and Valavanis in [24].

The 2D thermal profile of the longitudinal cross-section of the device was computed using COMSOL Multiphysics [25]. A heat sink temperature of 10 K and an insulated boundary condition surrounding the device was used to estimate the lattice temperature within each of the lasing and tuning cavities for different driving conditions. For simplicity, the input electrical power supplied to each section was assumed to be dissipated as heat. The peak power (pulse width) supplied to the lasing cavity (P_{Lasing}) and the tuning cavity (P_{Tuning}) were varied in the range 0–6 W (2 μs pulses) and 0–8 W (20–95 μs pulses), respectively. Typical temporal variations of the lattice temperatures predicted at the center of the lasing and tuning cavities are shown in Fig. 2(b). In this example, $P_{\mathrm{Lasing}} = 4$ W and $P_{\mathrm{Tuning}} = 5$ W, with tuning current pulse widths of both 20 μs (blue) and 95 μs (red). As can be seen, increasing the width of the tuning pulse from 20 μs to 95 μs not only increases the peak lattice temperature in the tuning cavity from ~56 K to ~73 K, but also increases the peak lattice temperature in the lasing cavity from ~46 K to ~52 K. Indeed, an increase in lattice temperature is predicted for both cavities as the pulse width supplied to the tuning cavity is increased [Fig. 2(c)]. A similar analysis was performed for different pulse amplitudes supplied to each cavity, for both cases of 20-μs-wide and 95-μs-wide current pulses supplied to the tuning cavity.

The changes in the lattice temperatures simulated from the thermal model were then translated to index perturbations in both the cavities, assuming a tuning coefficient of $\mathrm{d}n/\mathrm{d}T = 9.5 \times 10^{-5}$ K^{-1}. Finally, the spectral behavior of the device was calculated using the same transfer matrix approach described previously, and the results are shown in Fig. 2(d). Continuous tuning of the CC modes is predicted, with frequency tuning of <1 GHz (mode 1), ~1 GHz (mode 2), ~3 GHz (mode 2') and ~5 GHz (mode 3′), for P_{Tuning} in the range 0–8 W.

Optics EXPRESS

Additionally, P_{Lasing} was also varied (with electrical powers 3–6 W from a 2-µs-wide pulse train; corresponding to the operating dynamic range of the device) to introduce an additional index perturbation in the lasing cavity. For simplicity, the gain bandwidth of the QCL material was assumed to be invariant as a function of drive current. In this case, continuous tuning of ~6 GHz and ~3 GHz is predicted for CC modes at 2.245 THz (mode 1) and 2.254 THz (mode 3′), respectively, from 95-µs-wide P_{Tuning} pulse train, as shown in Fig. 2(e).

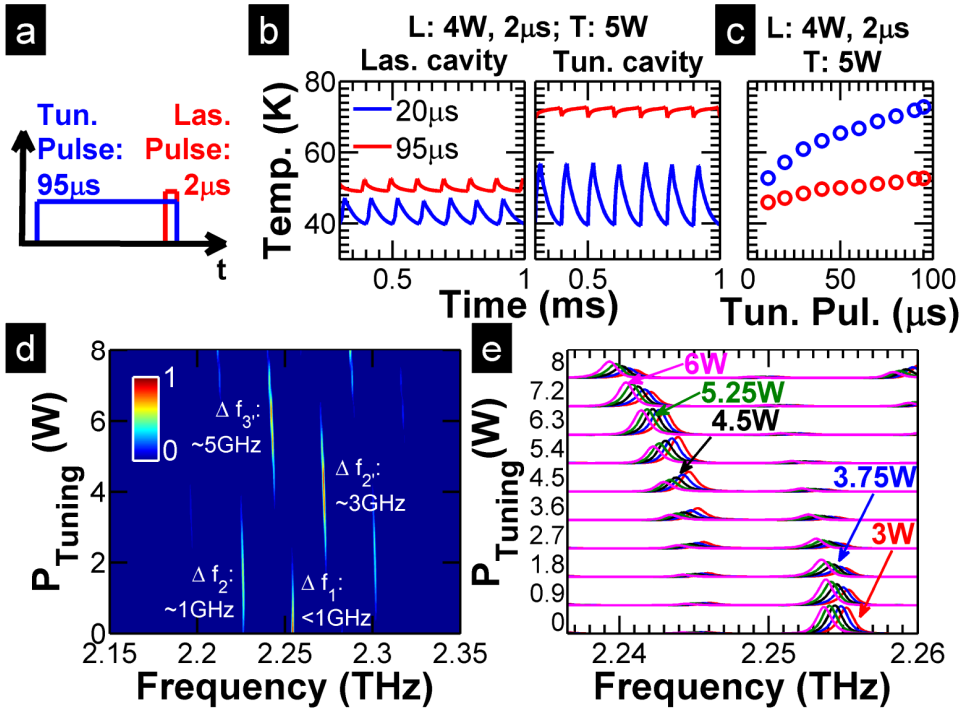

Fig. 2. (a) Schematic of the synchronization of the electrical pulses used to drive the lasing (red) and the tuning (blue) cavities. (b) Simulated temporal variation of the lattice temperature in the lasing and the tuning cavities for 2-µs-wide lasing pulses (P_{Lasing} = 4 W), and both 20-µs and 95-µs-wide tuning pulses (P_{Tuning} = 5 W). (c) Peak lattice temperature simulated at the center of the lasing (red) and the tuning (blue) cavities as a function of the width of pulses supplied to the tuning cavity. (d) Simulated discrete tuning (mode hopping) when the lasing cavity is driven with 2-µs-wide pulses (P_{Lasing} = 4.5 W) and the tuning cavity is driven with 95-µs-wide pulses, as a function of P_{Tuning}. (e) Simulated continuous tuning of the CC modes between 2.235 and 2.260 THz for combinations of different P_{Tuning} (95-µs-wide 0-8 W; y-axis) and the P_{Lasing} (3-6 W; colored spectra).

3. Fabrication and experimental results

A THz QCL based on a bound-to-continuum active region [26] was grown in the $Al_{0.1}Ga_{0.9}As$/GaAs material system using molecular beam epitaxy. Samples were processed into single-plasmon waveguides with 150-µm-wide and 14-µm-thick laser ridges. A 4.81-mm-long laser ridge was cleaved and mounted on a copper block. Subsequently, focused-ion beam (FIB) milling was used to divide the ridge into lasing and tuning cavities with lengths 3.50 mm and 1.31 mm, respectively. The device was mounted in a Janis ST-100 continuous-flow helium-cooled cryostat, and the lasing and tuning sections were driven with 2-µs (10 kHz), and 20-µs or 95-µs-wide (10 kHz) current pulses, respectively. Light–current–voltage (LIV) characteristics of the device were obtained by driving the lasing section only [Fig. 3(a)], and spectra were acquired using a Bruker Fourier transform infra-red spectrometer with resolution 7.5 GHz. THz radiation was collected from the front facet of the lasing section.

Optics EXPRESS

Initially, emission spectra were acquired with P_{Lasing}~4.10 W (laser drive current, I_{Lasing} = 0.95 A), for varying peak powers of the 95-µs-wide pulses supplied to the tuning cavity [Fig. 3(b)]. Discrete tuning (mode hops 1-2-2'-B-3′) with both red shift (modes 1-2, and 2' through to 3′) and blue shift (modes 2-2') in frequency was observed as P_{Tuning} is varied between 0 and 7.8 W, agreeing closely with the trend predicted in Fig. 1(c) and Fig. 2(d). We note that there is an additional mode hope from 2.218 THz (mode 2) to 2.208 THz, with a frequency separation of ~F_l. This mode hop can be explained by off-resonance conditions in the CC QCL design as shown in Fig. 1(b) iii, and a red-shift of such off-resonance conditions to the next transmission peak of the lasing cavity. We also note that whereas the transmission peaks were simulated to be at 2.254, 2.225, 2.270 and 2.245 THz [modes 1, 2, 2', and 3′ in Fig. 1(c)], emission were experimentally recorded at 2.251, 2.218, 2.285 and 2.241 THz [modes 1, 2, 2', and 3′ in Fig. 3(b)]. This slight disagreement between the simulation and experimental results may arise due to the FIB milling process resulting in minor variations of the cavity lengths. Furthermore, a narrow-band quasi-continuous tuning between commensurate CC modes B–3′ is observed due to a greater thermal perturbation in the lasing cavity owing to the wider heating pulses supplied to the tuning section. Indeed, mode B can be tuned continuously by ~5 GHz for P_{Tuning}~3.5−5 W, agreeing closely with the continuous tuning of ~5 GHz simulated in Fig. 2(d), before hopping by ~−13 GHz [to mode 3′ in Fig. 3(b)] at P_{Tuning} >5 W. As such, ΔF is observed to be ~−34 GHz (modes 1-2), ~−13 GHz (modes B-3′) and ~68 GHz (modes 2-2'). These variations in the values of ΔF as well as the blues shift from mode 2-2' can be attributed to the low F_r/F_{gain} in the CC design. We also note that additional weaker emission peaks (side modes) are observed at ~2.175 THz, ~2.21 THz and ~2.22 THz, for P_{Tuning} ~2.8–7.5 W, which can be assigned to off-resonance CC modes.

In order to evaluate the full spectral coverage achieved from this device, we also recorded emission spectra for different laser drive currents (within the 0.85−1.20 A operating dynamic range of the device) as a function of P_{Tuning} (using both 20 and 95-µs-wide tuning pulses). The spectral coverage obtained from all measurements showing single mode emission in the range ~2.185–2.285 THz is shown in Fig. 3(c). Additionally, through such concurrent control of both the laser driving current and tuning power, the modes centered at ~2.250 THz, 2.220 THz and 2.285 THz can be tuned quasi-continuously by ~7 GHz, 5 GHz and 4 GHz, respectively [Fig. 3(c) inset]. We note that a programmable frequency-selection scheme could readily be implemented through appropriate selection of input power to the two cavities. Alternatively, the device could be operated in a quasi-broadband regime through the use of a pseudo-random input waveform. Also, we note that the SMSR of these modes varies typically between 14 and 40 dB. This low value is due to the trade-off between achieving wide tunability whilst suppressing emission of multiple modes in these CC devices. We also note that whilst the output THz power does not degrade significantly as a function of the tuning power [17], variation of the laser drive current results in a change in the THz output power as shown in Fig. 3(a). As such, the quasi-continuous tuning of the CC modes also results in a variation of the output power from the CC QCL.

Optics EXPRESS

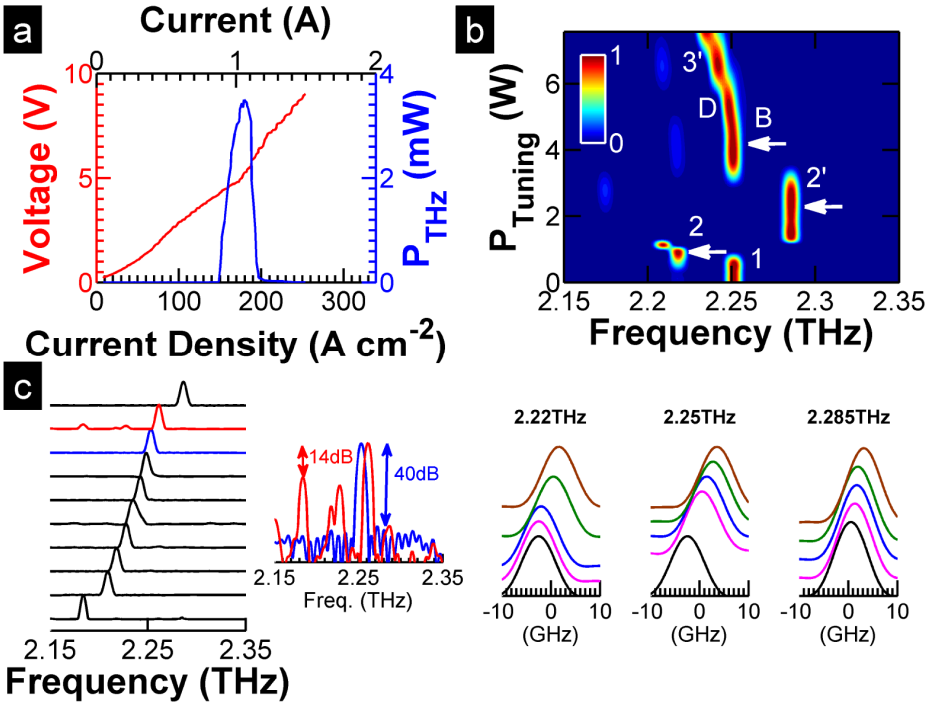

Fig. 3. Experimental data obtained at a heat sink temperature of 6 K: (a) LIV (peak THz power) characteristics of the lasing section with the tuning section grounded. THz radiation is collected from the front facet of the lasing section. (b) Experimentally observed spectra when the lasing cavity is driven with 2-µs-wide pulses (peak power 4.1 W), and the tuning cavity is driven with 95-µs-wide pulses. (c) Spectral coverage of the device with discrete frequency tuning extending from 2.185 to 2.285 THz. Spectra have been normalized and offset. (Inset): SMSR from two representative spectral lines (red and blue), and quasi-continuous tuning of ~5, 7, and 4 GHz centered at ~2.22, 2.25, and 2.85 THz respectively.

4. Continuous frequency tunable CC THz QCL

In order to achieve continuous frequency tuning of CC modes with a high SMSR, a one-dimensional photonic lattice (PL) was incorporated in the lasing cavity to introduce a photonic stopband in the emission spectra. Although this stopband suppresses discrete frequency tuning (mode hopping) in these devices, it can enhance the SMSR while retaining continuous tunability around the Bragg frequency of the PL. To this end, a one-dimensional finite PL [20] comprising ten defect sites and a central π-shift element [27] was incorporated in the center of the lasing cavity using FIB milling to an etch depth of ~1.9 µm [Fig. 4(a)]. The periodicity of the PL (Λ = 19.85 µm,) was matched to a Bragg frequency of 2.21 THz. The PL was designed with a stopband width of ~234 GHz, which was sufficient to suppress all previously accessible CC modes except those centered at the Bragg frequency [Fig. 4(b)]; PLs with an etch depth of ~2 µm were found by simulation to provide the desired refractive index contrast (Δn = 0.31) to achieve this wide stopband. The spectral emission of this device was simulated, using the transfer matrix model described previously, for the case of 95-µs-wide pulses supplied to the tuning cavity. As shown in Fig. 4(c), the PL was predicted to suppress all discrete frequency tuning simulated in Fig. 2(d); instead continuous tuning over ~5 GHz centered at ~2.215 THz was predicted. Experimental spectra acquired with 2-µs-wide current pulses I_{Lasing} = 1.10A (P_{Lasing} = 5.5 W) are shown in Fig. 4(c). An SMSR of 40 dB and continuous tuning over ~3 GHz were observed, in good agreement with the simulations. Furthermore, since the laser drive current is not varied in this case, continuous tuning is achieved without any degradation of the THz output power [Fig. 4(c) inset].

Optics EXPRESS

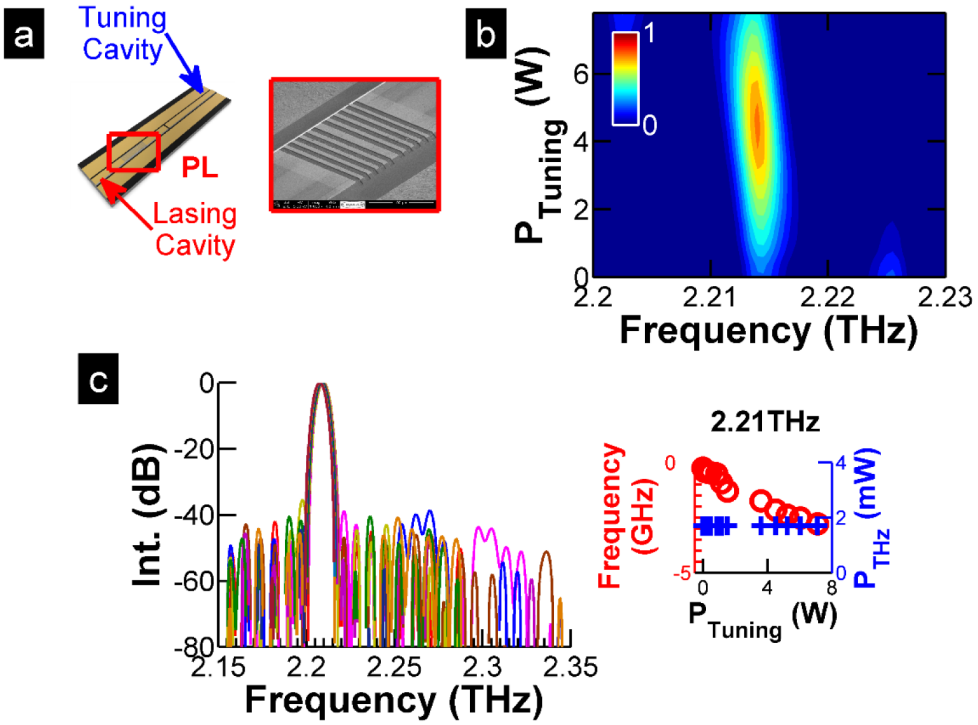

Fig. 4. (a) Illustration of a PL incorporated in the lasing cavity of the CC QCL. Inset: Scanning electron micrograph of the PL formed by focused-ion beam milling. (b) Simulated emission spectra of the CC device with PL, as a function of the peak electrical power supplied to the tuning cavity (95-μs-wide pulses) (c) Experimental spectra obtained at a heat sink temperature of 6 K showing an improved SMSR of 40 dB. Inset: Weighted mean of the spectral power distribution (red circle) and variation of output power from the lasing section (blue plus) as a function of the peak electrical power supplied to the tuning cavity.

5. Conclusions

In summary, an increase in the number of accessible modes in a CC THz QCL has been demonstrated by reducing the repetition frequency of the Vernier resonance and increasing the CSR of the CC design. This allowed both red shift and blue shift in frequency along with a controlled variation of the frequency separation between mode hops. Wide current pulses are used to drive the tuning cavity to introduce a greater thermal perturbation in the lasing cavity section via heat conduction through the monolithic substrate enabling a narrow band quasi-continuous tuning. A spectral coverage range of ~100 GHz from 2.185 to 2.285 THz and a quasi-continuous tuning of ~7 GHz at ~2.25 THz was realized using this scheme. The SMSR was improved by patterning a PL into the lasing cavity, and a continuous tuning of ~3 GHz with an SMSR of 40 dB was recorded, without any degradation in output power. We note that frequency tunability could be further optimized by using an active region design with a larger gain bandwidth and better dynamic range.

Funding

Engineering and Physical Sciences Research Council (EPSRC), UK (COTS programme EP/J017671/1, and EP/J002356/1). EHL and AGD are grateful for support from the Royal Society and Wolfson Foundation.

Optics EXPRESS

Acknowledgments

Research data associated with this paper are openly available from the University of Leeds data repository: http://doi.org/10.5518/115.